Power Engineering and Engineering Thermophysics
https://www.acadlore.com/journals/PEET

Influence of Cooling and Lubrication Parameters on Robot Bone Grinding Temperature and Prediction Modeling

Heqiang Tian[1*], Bin Tian[1], Debao Meng[1], Qian Xu[1], Xiaoqing Dang[2]

[1] College of Mechanical and Electronic Engineering, Shandong University of Science and Technology, 266590 Qingdao, China
[2] Qingdao Municipal Hospital, 266073 Qingdao, China

[*] Correspondence: Heqiang Tian (tianhq26@sdust.edu.cn)

Received: 01-01-2023 **Revised:** 02-11-2023 **Accepted:** 03-09-2023

Citation: H. Q. Tian, B. Tian, D. B. Meng, Q. Xu, and X. Q. Dang, "Influence of cooling and lubrication parameters on robot bone grinding temperature and prediction modeling," *Power Eng. Eng. Thermophys.*, vol. 2, no. 1, pp. 26-41, 2023. https://doi.org/10.56578/peet020103.

Abstract: In the process of robot bone grinding, a large amount of heat is generated, which will cause mechanical and thermal damage to bone tissues and nerves. It is necessary to study the influence of cooling and lubrication parameters on the robot bone grinding temperature and establish the prediction models among them. The FE model of single abrasive bone grinding was established to explore the influence of cooling and lubrication parameters on the bone grinding temperature. Response surface design of experiment was carried out to obtain the simulation results, and Design-Expert was used to establish a multiple regression prediction models of grinding temperature under the condition of different cooling and lubrication. Through the variance and response surface comparative analysis of the prediction model, the influence rules of the bone grinding parameters and the cooling and lubrication parameters on the bone grinding temperature was obtained. A robot bone grinding experiment was performed to prove the accuracy of FE simulation and prediction model. The research results show that the relationship between grinding temperature and cooling lubrication parameters obtained by FE simulation, RSM prediction and experiment verification is consistent, and the simulation model and prediction model of cooling and lubrication parameters are proven to be correct and effective. The influence rules and prediction effects obtained in this study will provide a reasonable scheme for doctors to implement robot bone grinding with high efficiency and low damage, and establish the theoretical basis for the effective control of robot bone grinding force thermal damage.

Keywords: Bone grinding; Cooling lubrication; FE simulation; Grinding temperature; Prediction modeling

1. Introduction

In recent years, a robot is widely used in bone surgery to grind the bone into the shape required [1, 2]. However, the bone material is an anisotropic and heterogeneous composite material with different bone structures, and bone cells are very sensitive to temperature and will lose biological activity under the influence of high temperature, that is, heat necrosis, and excessive grinding force will cause the fracture of bone canal, resulting in loss of the ability to recover and regenerate [3]. Therefore, how to reduce the force and heat damage of bone tissue grinding is very important in the process of robot bone tissue grinding surgery. At present, scholars have conducted a lot of cutting experiments on bone tissue, providing a lot of experience and conclusions on cutting force and heat of bone tissue [4]. However, most of the previous studies on the mechanism of bone tissue cutting did not consider the problem of cooling and lubrication, which is quite different from the actual surgical bone tissue cutting conditions. Cooling and lubrication can better optimize the tribological performance between bones and tools, and can reduce the heat generated in the cutting process, and is one of the most important factors to reduce the temperature in bone cutting [5].

Augustin et al. [6] studied the temperature change of cortical bone drilling with step drills under different cooling conditions of internal cooling and external cooling, and found that both internal cooling and step drills can significantly reduce the temperature. Kirschner and Meyer [7] found that the greater the flow of normal saline, the

better the cooling effect, and preliminarily revealed the relationship between the flow of normal saline and temperature changes, when studying internally cooled dental drilling. Gholampour and Deh [8] and Hassanalideh and Gholampour [9] analyzed and compared the temperature drop of non-cooling, general water cooling, and internal gas cooling, then found that gas cooling could greatly reduce the drilling temperature of cortical bone, and the changes of temperature and axial force at different drilling angles from radial to axial. Kondo et al. [10] studied cool methods of bone grinding surface temperature to reduce high temperature diffusion under different grinding methods by drip irrigation of medical physiological saline. Shin and Yoon [11] studied the cooling performance of medical saline spray cooling system, which can reduce the grinding heat by 14%~30%, compared with the cooling system of drip irrigation medical saline. Yang et al. [12] studied temperature cooling effect of bone micro-grinding under the different conditions, such as dry grinding, drop cooling, spray cooling and nano-particle spray cooling, and the results showed that nano-particle spray cooling was the best, followed by spray cooling, drop cooling and dry grinding.

The grinding fluid for cooling and lubrication by increasing the convection heat transfer coefficient and reducing the friction coefficient, can reduce the grinding temperature and the mechanical-thermal damage in the process of bone grinding. In order to reduce the secondary damage to human bone tissues caused by grinding temperature during robotic bone grinding surgery, this paper uses simulation and experimental methods in turn to study the cooling and lubrication mechanism and predictive modeling of robotic bone grinding, explore the rules and effects of robotic bone grinding cooling and lubrication, which will provide a reasonable scheme for doctors to implement robotic bone grinding with high efficiency and low damage, and establish the theoretical basis for the effective control of robot bone grinding force thermal damage.

2. Materials and Methods

2.1 FE Model of Single Abrasive Bone Grinding

The abrasive tool commonly used in bone grinding surgery is a high speed spherical grinding head. Grinding is a process in which countless abrasive particles on the surface of the spherical grinding head act together on the workpiece. In order to facilitate the study of bone grinding laws, the abrasive particles are simplified as cone shape in this paper, as shown in Figure 1.

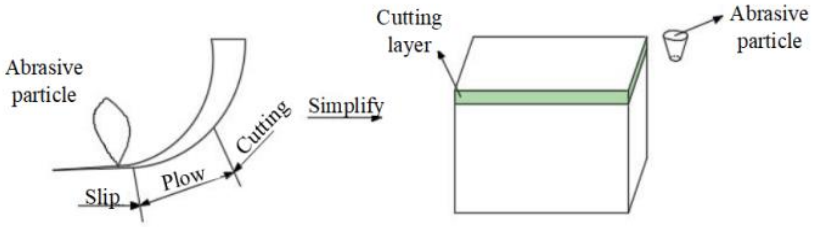

Figure 1. Simplified model of bone grinding simulation

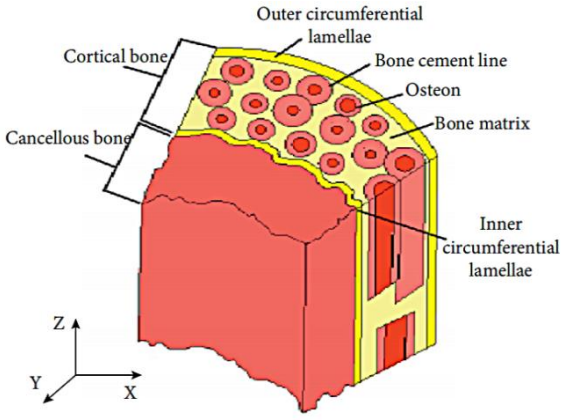

Figure 2. Microstructure of bone

Bones can be divided into cortical and cancellous bones based on their density and structure. As shown in Figure 2, cortical bone and cancellous bone are two different tissues. According to the grinding direction of the abrasive particles and the direction of the bone unit, the cutting modes can be divided into vertical direction, parallel

direction, and cross direction. In our early research [13, 14], it was found that the grinding temperature and grinding force in the vertical direction are the largest among the three cutting modes, followed by the cross direction, and the grinding temperature and grinding force in the parallel direction are the smallest. In order to explore the cooling and lubricating effect of coolant on bone grinding temperature, the grinding direction selected in FE simulation is the vertical direction with the largest grinding temperature shown in Figure 3(a). Because cortical bone structure is different from traditional grinding workpiece, it determines the anisotropy of bone structure [15]. It is impossible to obtain complete anisotropic mechanical parameters, and so proper simplification of the mechanical parameters is required to establish the finite element simulation model [16]. ABAQUS was used to simulate the grinding temperature under different cooling and lubrication conditions by changing the convective heat transfer coefficient and friction coefficient in the simulation. The material property parameters of the tool, matrix, and bone unit are shown in Table 1.

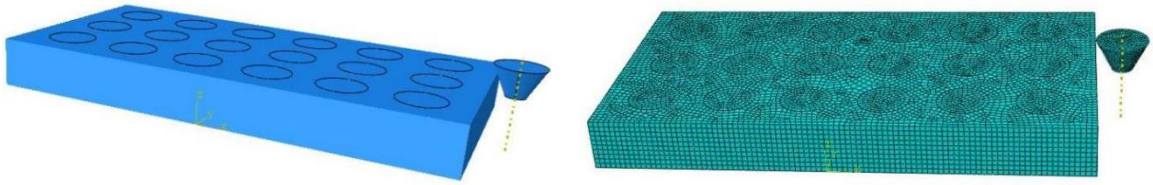

(a) Model of vertical direction (b) Mesh model

Figure 3. Finite element simulation model of single abrasive bone grinding

Table 1. Material properties of cutting tools and bone

Content	Density (kg/m^3)	Young's modulus (GPa)	Poisson's ratio	Coefficient of thermal conductivity (W/m·K)	Specific heat capacity (J/(kg·°C))
Cutter	7800	200	0.25	25.2	460
Matrix	1700	26.3	0.3	0.53	1260
Bone unit	1800	20	0.3	0.55	1260

In the simulation model, the tool surface is set as the first surface, the node set established in the cutting area is set as the slave surface, the constraint enhancement method is selected as the kinematic contact method, the sliding formula is selected as the finite sliding formula, and the contact control is set as the default item. In the tangential behavior, the friction formula is selected as the penalty function, the elastic sliding and shear stress are set as the default values, the friction coefficient is set as 0.6, and the initial temperature is set as 25 ℃. In the normal behavior, the pressure interference is set to "hard" contact, and the constraint execution method is set to default. The tool model is defined as a rigid body, the reference point is set on the tool, and coupling constraints are added to the tool model to directly apply the motion load conditions to the reference point. In the process of analysis, it was found that the mesh of bone unit and matrix was larger than 0.06 mm, and the analysis accuracy was affected. Better results can be obtained by controlling the mesh size of bone unit and matrix part within 0.06 mm. Sweeping mesh generation technology shall be adopted, and the mesh type shall be set as hexahedron. The tool mesh is divided freely, and the mesh type is set as tetrahedron. The established FE simulation model of single abrasive bone grinding by ABAQUS is shown in Figure 3(b). In order to make the results more accurate, this section uses the method of controlling a single variable to analyze the change rules of grinding temperature with different convective heat transfer coefficient and friction coefficient.

During cortical bone cutting, the change of cortical bone belongs to high strain rate deformation, and the cutting force is nonlinear, so Johnson-Cook model is selected as the constitutive model, which shows good ability to describe the elastic-plastic behavior of cortical bone [17]. The mathematical expression of Johnson-Cook model is shown as follows:

$$\sigma = (A + B\varepsilon^n)(1 + C\ln\dot{\varepsilon})\left(1 - T^{*m}\right) \tag{1}$$

where, σ represents total flow stress, ε represents equivalent plastic strain, $\dot{\varepsilon}$ represents strain rate, A is yield stress, B is machining hardening modulus, C represents strain rate sensitivity coefficient, m represents temperature sensitivity coefficient, n represents hardening coefficient, and T^* represents relatively stable temperature. The parameters in the Johnson-Cook model are shown in Table 2.

Table 2. Parameters in the Johnson-Cook model

A (MPa)	B (MPa)	n	C	m	T^* (°C)
50	101	0.08	0.03	1.03	875

The equivalent plastic strain criterion is selected as the bone chip separation criterion. The expression in Johnson-Cook model is shown as follows:

$$\varepsilon_f = \left[d_1 + d_2 \exp\left(d_3 \frac{\sigma_p}{\sigma_s} \right) \right] \left[1 + d_4 \ln\left(\frac{\dot{\varepsilon}_p}{\dot{\varepsilon}_0} \right) \right] \left[1 + d_5 \left(\frac{T - T_{melt}}{T_{melt} - T_{room}} \right) \right] \tag{2}$$

where, d_1-d_5 represents failure parameter of processed material, ε_f represents failure strain, σ_p represents compressive stress, σ_s represents equivalent stress, $\dot{\varepsilon}_p$ represents strain rate, and $\dot{\varepsilon}_0$ represents reference strain rate.

2.2 Response Surface Design of Experiment of FE Simulation

Response surface method (RSM) is a mathematical-statistical method used to model and analyse the mathematical relationship between the design variables and the responses, which consists of experimental design and functional fitting [18]. It is necessary to determine factors and levels, select experimental design methods, obtain experimental results, analyze experimental data, fit selected models, and analyze the effectiveness of models. The experimental design method has the advantages of less times of experiments, high predictability, intuitively selecting the best value range from the effect surface, and good experimental optimization effect [19]. The quadratic regression equation considering the factors and effective interactions can be written as [4, 20]:

$$y = \beta_0 + \sum_{i=1}^{k} \beta_i x_i + \sum_{i=1}^{k} \beta_{ii} x_i^2 + \sum_{i} \sum_{j} \beta_{ij} x_i x_j + \varepsilon \tag{3}$$

where, y is the response function, β is the regression coefficient matrix, x representing all influencing factors, and ε is an error item.

The second order response surface central composite design (CCD) was used for experiment design. The regression equation of grinding temperature under different cooling conditions was established by regression analysis. The factors of the regression equation were rotating speed, feed speed, grinding thickness, convective heat transfer coefficient and friction coefficient. The regression equation of grinding temperature without cooling mode includes three factors: rotating speed, feed speed and grinding thickness. The regression equation of grinding temperature with different cooling modes includes five factors: rotating speed, feed speed, grinding thickness, convection heat transfer coefficient and friction coefficient. Table 3 shows the grinding parameters factors and their level range of variation based on three coded units.

Table 3. Grinding parameters factors and level range of variation based on three coded units

Factors	-1	0	1
Rotating speed n (r/min)	3000	4500	6000
Feed speed v_f (mm/s)	1	3.5	6
Grinding thickness a_p (mm)	0.1	0.25	0.4
Convective heat transfer coefficient	1000	1500	2000
Friction coefficient	0.3	0.4	0.5

2.3 Experiment Method of Verification

A six-axis robot installed with a stainless steel spherical grinding head having a diameter of 4 mm was used to carry out bone grinding verification experiments. A K-type dual-channel thermocouple thermometer with the measurement range -50~1300℃, the measurement resolution 0.1℃, and the measurement accuracy ± [0.5% rdg+1℃] was selected for temperature measurement. Figure 4 illustrates the robot bone grinding experiment set-up.

As the composition of cow bone is basically the same as that of human bone, cow bone is selected as the experimental bone in this paper. As shown in Figure 5, the cow femur was polished to obtain several bone pieces. Due to the poor physiological activity of dense bone, the mechanical properties of cortical bone would not be affected if it was kept in the freezing environment of -20℃. Therefore, in order to ensure the accuracy of the experiment, it is necessary to ensure the freshness of the bovine femur. Therefore, after the preparation of the bone pieces, they were placed in a cold storage environment of -20℃ to keep water for the experiment.

The experiment was divided into two groups: dry grinding and grinding with cooling fluid. To ensure the experiment accuracy, all experiments were carried out at room temperature, and each experiment was repeated for three times. During the experiment process, the cooling fluid was continuously injected into the grinding surface

of bone blocks. K type thermocouple was used to measure the grinding temperature in the process of bone grinding, and the grinding temperature obtained in the experiment was recorded. In order to eliminate the interference in the experiment, the grinding temperature is the average of the maximum grinding temperature in the three experiments. The bone grinding modes were shown in Figure 6.

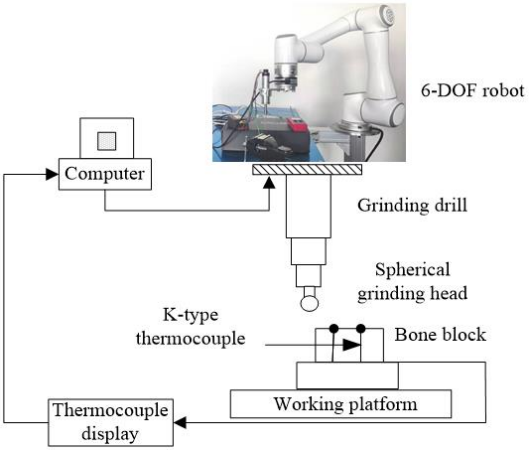

Figure 4. Robot bone grinding experiment system

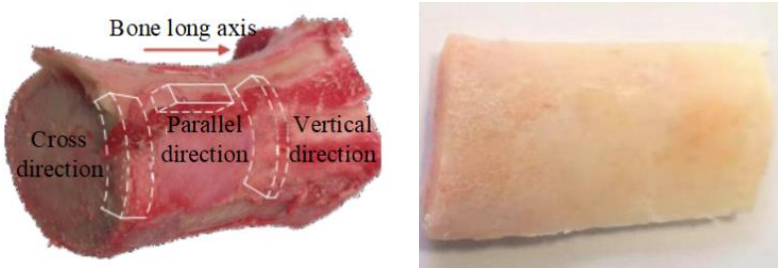

(a) Cutting direction (b) Bone block

Figure 5. Preparation process of bone blocks

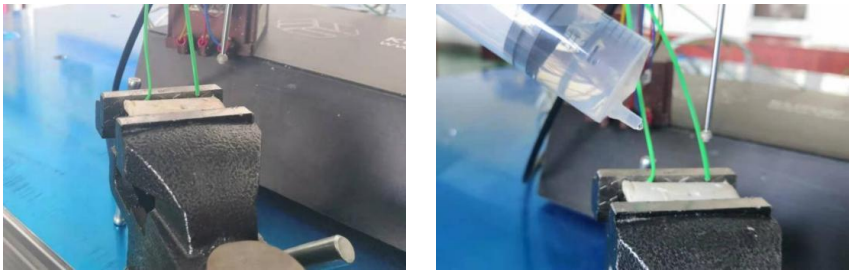

(a) Dry grinding (b) Grinding with cooling fluid

Figure 6. Bone grinding modes

3. Results and Discussion

3.1 Influence of Cooling and Lubricating Parameters on Bone Grinding Temperature

In order to explore the influence of convection heat transfer coefficient on bone grinding temperature, the convection heat transfer coefficient was changed by controlling other grinding factors unchanged in this bone grinding simulation. The rotating speed was 3000r/min, the feed speed was 2mm/s, the grinding thickness was 0.1mm, the friction coefficient was 0.4, and the convective heat transfer coefficient was set to 500, 1000, 1500, 2000 and 2500 respectively. The grinding temperature after reaching the stable grinding state under each convective heat transfer coefficient was recorded. As shown in Figure 7, as the convective heat transfer coefficient increases, the grinding temperature tends to decrease, indicating that the greater the convective heat transfer coefficient, the more significant cooling effect on bone grinding.

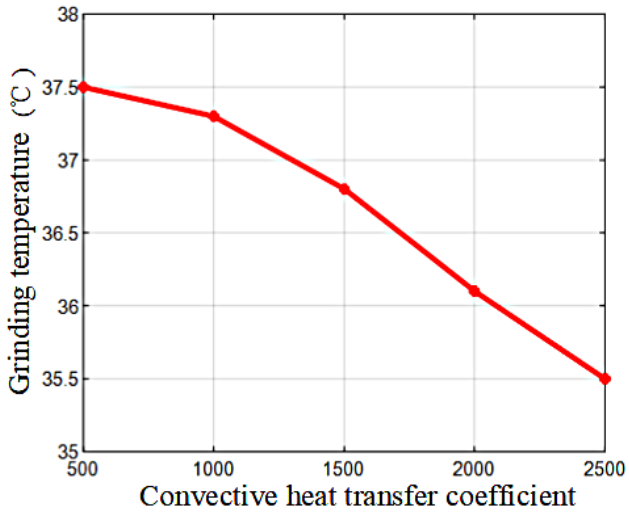

Figure 7. Relationship between convective heat transfer coefficient and grinding temperature

In order to explore the influence of friction coefficient on grinding temperature, the friction coefficient was changed by controlling other grinding factors unchanged in this simulation. The rotating speed was controlled at 3000r/min, the feed speed was 2mm/s, the grinding thickness was 0.1mm, and the convective heat transfer coefficient was 1500. The friction coefficients in the simulation were changed to 0.2, 0.3, 0.4, 0.5 and 0.6 respectively, and the grinding force after reaching the stable grinding state under each friction coefficient was recorded. Although, the effect of friction coefficient on grinding temperature cannot be decoupled from other grinding factors and friction coefficient, as the friction coefficient increases, the grinding temperature tends to increase, generally speaking that the smaller the friction coefficient, the more significant cooling effect on bone grinding, as shown in Figure 8.

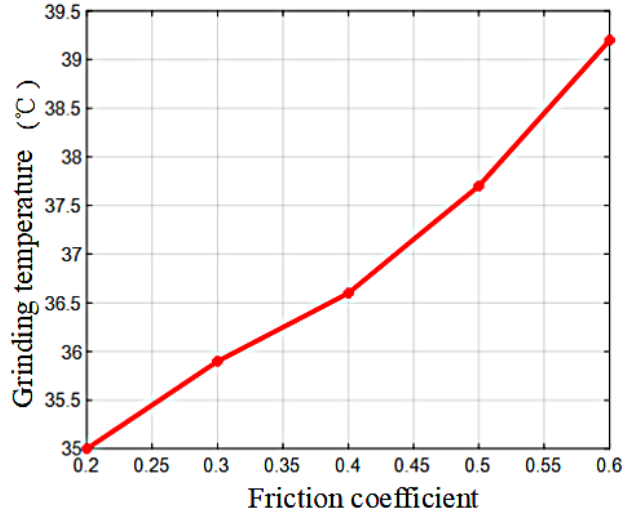

Figure 8. Relationship between grinding temperature and friction coefficient

3.2 Simulation Data of Bone Grinding Temperature

The output variable T_1 for 20 experiments represented the grinding temperature without grinding fluid, and the dry grinding test grouping and test arrangement order were presented in Table 4. The output variable T_2 for 82 experiments represented the grinding temperature with grinding fluid, and the test grouping and experiment arrangement order for different cooling methods were presented in Table 5. Using the simulation model of single-abrasive bone grinding temperature established above, the bone grinding simulation was performed in sequence according to the simulation order of Table 4 and Table 5, and the simulation results were filled in the tables respectively.

Table 4. Arrangement of simulation sequence and data results without grinding fluid

Serial number	Simulation order	Rotating speed n (r/min)	Feed speed v_f (mm/s)	Grinding thickness a_p (mm)	Temperature T_1(℃)
9	1	3000	3.50	0.17	38
4	2	6000	6.00	0.10	39
7	3	3000	6.00	0.25	43
8	4	6000	6.00	0.25	47
18	5	4500	3.50	0.17	42
10	6	6000	3.50	0.17	47
12	7	4500	6.00	0.17	39
11	8	4500	1.00	0.17	54
15	9	4500	3.50	0.17	45
20	10	4500	3.50	0.17	45
13	11	4500	3.50	0.10	41
1	12	3000	1.00	0.10	44
3	13	3000	6.00	0.10	26
5	14	3000	1.00	0.25	47
16	15	4500	3.50	0.17	42
14	16	4500	3.50	0.25	45
2	17	6000	1.00	0.10	52
19	18	4500	3.50	0.17	45
6	19	6000	1.00	0.25	55
17	20	4500	3.50	0.17	42

Table 5. Grinding simulation sequence arrangement and data results of different cooling modes

Serial number	Simulation order	Rotating speed n (r/min)	Feed speed v_f (mm/s)	Grinding thickness a_p (mm)	Convective heat release coefficient	Friction coefficient	Temperature T_2(℃)
65	1	3000	3.5	0.17	1500	0.4	36
44	2	6000	1	0.25	1000	0.5	53
53	3	3000	6	0.1	2000	0.5	25.5
47	4	6000	6	0.25	1000	0.5	47.1
4	5	6000	1	0.1	1000	0.3	49
27	6	6000	1	0.25	2000	0.3	50.4
19	7	6000	1	0.1	2000	0.3	47.7
46	8	3000	6	0.25	1000	0.5	41.3
16	9	6000	6	0.25	1000	0.3	46
75	10	4500	3.5	0.17	1500	0.4	40
20	11	6000	1	0.1	2000	0.3	47.7
51	12	6000	1	0.1	2000	0.5	49
70	13	4500	3.5	0.25	1500	0.4	44
52	14	6000	1	0.1	2000	0.5	49
54	15	3000	6	0.1	2000	0.5	25.5
73	16	4500	3.5	0.17	1500	0.3	39.5
67	17	4500	1	0.17	1500	0.4	50.9
48	18	6000	6	0.25	1000	0.5	47.1
36	19	6000	1	0.1	1000	0.5	50.1
23	20	6000	6	0.1	2000	0.3	36.1
69	21	4500	3.5	0.1	1500	0.4	50.9
7	22	6000	6	0.1	1000	0.3	36.7
72	23	4500	3.5	0.17	2000	0.4	39.5
9	24	3000	1	0.25	1000	0.3	43
74	25	4500	3.5	0.17	1500	0.5	40.5
59	26	6000	1	0.25	2000	0.5	51.8
62	27	3000	6	0.25	2000	0.5	40.2
50	28	3000	1	0.1	2000	0.5	42
30	29	3000	6	0.25	2000	0.3	39
58	30	3000	1	0.25	2000	0.5	42.9
77	31	4500	3.5	0.17	1500	0.4	40
14	32	3000	6	0.25	1000	0.3	39.9
81	33	4500	3.5	0.17	1500	0.4	40
32	34	6000	6	0.25	2000	0.3	45
82	35	4500	3.5	0.17	1500	0.4	40
5	36	3000	6	0.1	1000	0.3	25.4

Table 5. Grinding simulation sequence arrangement and data results of different cooling modes(continued)

Serial number	Simulation order	Rotating speed n (r/min)	Feed speed v_f (mm/s)	Grinding thickness a_p (mm)	Convective heat release coefficient	Friction coefficient	Temperature T_2(℃)
61	62	3000	6	0.25	2000	0.5	40.2
43	63	6000	1	0.25	1000	0.5	53
71	64	4500	3.5	0.17	1000	0.4	44
64	65	6000	6	0.25	2000	0.5	46.2
57	66	3000	1	0.25	2000	0.5	42.9
35	67	6000	1	0.1	1000	0.5	50.1
76	68	4500	3.5	0.17	1500	0.4	40
37	69	3000	6	0.1	1000	0.5	26.5
49	70	3000	1	0.1	2000	0.5	42
80	71	4500	3.5	0.17	1500	0.4	40
29	72	3000	6	0.25	2000	0.3	39
66	73	6000	3.5	0.17	1500	0.4	44.7
18	74	3000	1	0.1	2000	0.3	40.9
33	75	3000	1	0.1	1000	0.5	43.1
55	76	6000	6	0.1	2000	0.5	37.5
60	77	6000	1	0.25	2000	0.5	51.8
39	78	6000	6	0.1	1000	0.5	38
11	79	6000	1	0.25	1000	0.3	51.6
21	80	3000	6	0.1	2000	0.3	25.1
40	81	6000	6	0.1	1000	0.5	38
13	82	3000	6	0.25	1000	0.3	39.9
34	37	3000	1	0.1	1000	0.5	43.1
78	38	4500	3.5	0.17	1500	0.4	40
12	39	6000	1	0.25	1000	0.3	51.6
41	40	3000	1	0.25	1000	0.5	44.2
1	41	3000	1	0.1	1000	0.3	41.8
68	42	4500	6	0.17	1500	0.4	37.8
63	43	6000	6	0.25	2000	0.5	46.2
79	44	4500	3.5	0.17	1500	0.4	40
24	45	6000	6	0.1	2000	0.3	36.1
56	46	6000	6	0.1	2000	0.5	37.4
6	47	3000	6	0.1	1000	0.3	25.3
10	48	3000	1	0.25	1000	0.3	43
31	49	6000	6	0.25	2000	0.3	45
15	50	6000	6	0.25	1000	0.3	45.8
26	51	3000	1	0.25	2000	0.3	41.8
17	52	3000	1	0.1	2000	0.3	40.9
3	53	6000	1	0.1	1000	0.3	49
38	54	3000	6	0.1	1000	0.5	26.5
8	55	6000	6	0.1	1000	0.3	36.7
42	56	3000	1	0.25	1000	0.5	44.2
28	57	6000	1	0.25	2000	0.3	50.4
22	58	3000	6	0.1	2000	0.3	25.1
45	59	3000	6	0.25	1000	0.5	41.3
2	60	3000	1	0.1	1000	0.3	41.8
25	61	3000	1	0.25	2000	0.3	41.8

3.3 Prediction Model of Bone Grinding Temperature

Design-Expert is used to analyze the grinding temperature obtained from the simulation experiment. The reliability was set as 95%, and the significance level of statistical test was P<0.05. The regression equation prediction model for T_1 and the regression equation prediction model for T_2 can be obtained through regression analysis, as shown below.

$$T_1 = 43.63 + 4.2A - 5.8B + 3.5C + 0.13AB - 1.12AC + 2.38BC - 1.32A^2 + 2.68B^2 - 0.82C^2 \quad (4)$$

$$\begin{aligned} T_2 = {} & 41.34 + 4.15A - 4.65B + 3.2C - 0.54D + 0.59E + 0.21AB - 0.47AC + 0.044AE + 2.46BC \\ & + 0.097BD - 0.022BE - 0.059CD + 0.034CE - 0.031DE - 2.33A^2 + 1.67B^2 + 4.77C^2 - 0.93D^2 - 2.68E^2 \end{aligned} \quad (5)$$

where, A represents the rotating speed, B represents the feed speed, C represents the grinding thickness, D represents the convection heat transfer coefficient of grinding fluid, and E is the friction coefficient of grinding fluid.

In order to test the rationality of T_1 and T_2 prediction models, it is necessary to diagnose the prediction models. Design-Expert software can be used to fit T_1 and T_2 prediction models and point out the key items that must be retained in the model.

Table 6 is the analysis result of variance of T_1 regression equation by using ANOVA module of variance analysis in Design-Expert software. If $P<0.05$, it indicates that the obtained prediction model is significant at this level, otherwise it is not significant.

It can be seen from Table 6 that among the influencing factors of T_1 model, the rotating speed A, the feed speed B and the grinding thickness C are all significant, and the misfit term in the table is used to indicate the difference between the model and the simulation results degree, and $P>0.05$, the misfit term is not significant and there is no misfit factors, which is beneficial to the model, indicating that the prediction model can replace the simulation point to analyze the simulation results.

Table 6. Variance analysis of regression equation for T_1 prediction model

Factors	Sum of squares of deviations	Degrees of freedom	Mean square error	F	P	
Model	710.77	9	78.97	21.32	<0.0001	Significant
Rotating speed A	176.40	1	176.40	47.63	<0.0001	Significant
Feed speed B	336.40	1	336.40	90.84	<0.0001	Significant
Grinding thickness C	122.50	1	102.50	33.08	0.0002	Significant
AB	0.13	1	0.13	0.034	0.8579	
AC	10.12	1	10.12	2.73	0.1292	
BC	45.13	1	45.13	12.18	0.0558	
A^2	4.78	1	4.78	1.29	0.2825	
B^2	19.78	1	19.78	5.34	0.0534	
C^2	1.84	1	1.84	0.50	0.4969	
Residual	37.03	10	3.70			
Misfit term	23.53	5	4.71	1.74	0.2784	Not Significant
Pure error	13.50	5	2.70			

Table 7. Variance analysis of regression equation of T_2 prediction model

Factors	Sum of squares of deviations	Degrees of freedom	Mean square error	F	P	
Model	3768.59	20	188.43	60.48	< 0.0001	Significant
Rotating speed A	1135.03	1	1135.03	364.31	< 0.0001	Significant
Feed speed B	1428.95	1	1428.95	458.64	< 0.0001	Significant
Grinding thickness C	675.20	1	675.20	216.72	< 0.0001	Significant
Convection heat transfer coefficient D	19.09	1	19.09	6.13	0.0161	Significant
Friction coefficient E	23.28	1	23.28	7.47	0.0082	Significant
AB	2.81	1	2.81	0.90	0.3464	
AC	14.25	1	14.25	4.57	0.0365	Significant
AD	0.000	1	0.000	0.000	1.0000	
AE	0.12	1	0.12	0.039	0.8435	
BC	388.09	1	388.09	124.56	< 0.0001	Significant
BD	0.60	1	0.60	0.19	0.6622	
BE	0.031	1	0.031	9.830E-003	0.9213	
CD	0.031	1	0.031	0.072	0.7888	
CE	0.076	1	0.076	0.024	0.8767	
DE	0.063	1	0.063	0.020	0.8878	
A^2	13.45	1	13.45	4.32	0.0420	Significant
B^2	6.91	1	6.91	2.22	0.1414	
C^2	56.39	1	56.39	18.10	< 0.0001	Significant
D^2	2.14	1	2.14	0.69	0.4103	
E^2	17.79	1	17.79	5.71	0.0200	Significant
Residual	190.05	61	3.12			
Misfit term	190.02	22	8.64	11228.50	0.9895	Not Significant
Pure error	0.030	39	7.692E-004			

Table 7 is the analysis result of variance of T_2 regression equation by using ANOVA module of variance analysis in Design-Expert software. It can be seen from Table 7 that among the influencing factors of the T_2 model, the rotating speed A, the feed speed B, the grinding thickness C, the convective heat release coefficient D and the friction coefficient E are all significant, and P>0.05, the misfit term is not significant and there is no misfit factors, which is beneficial to the model, indicating that the prediction model can replace the simulation point to analyze the simulation results.

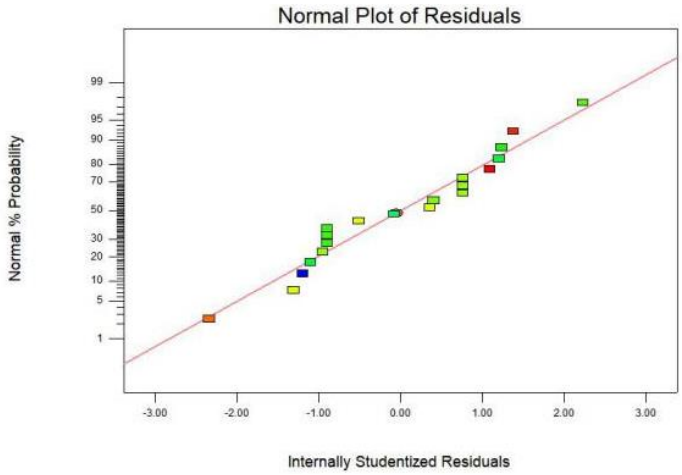

(a) Normal probability distribution of residuals for T_1 prediction model

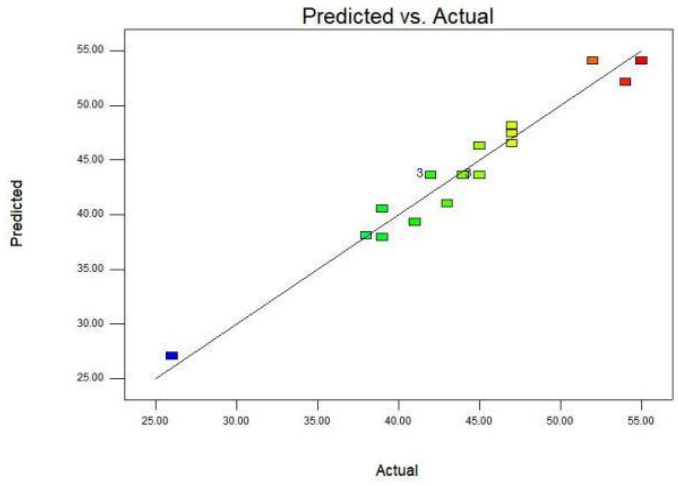

(b) A plot of the predicted value of T_1 versus the actual value of T_1

Figure 9. Residual analysis of T_1 regression equation

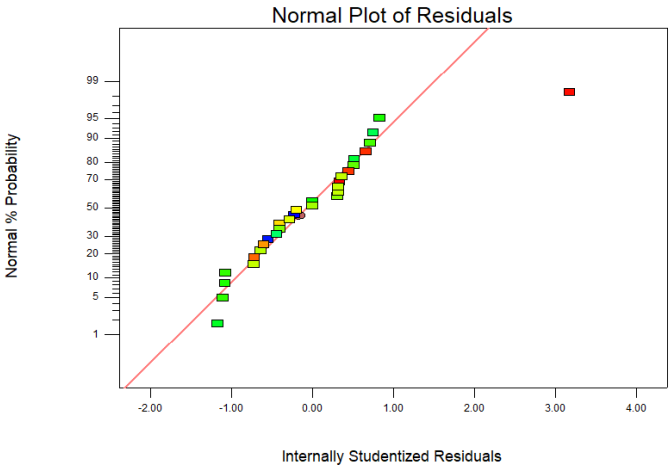

(a) Normal probability distribution of residuals for T_2 prediction model

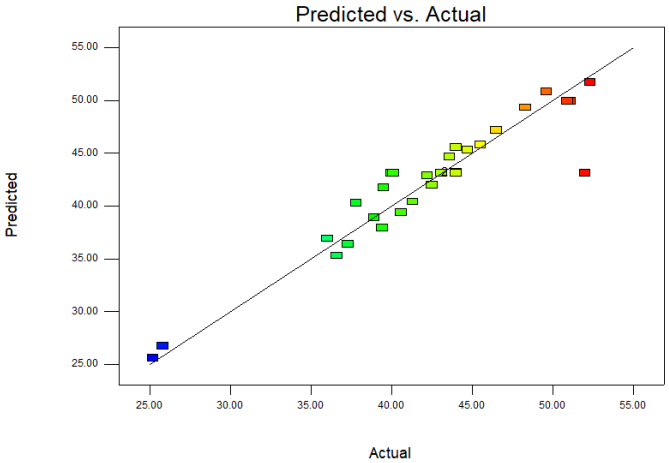

(b) A plot of the predicted value of T_2 versus the actual value of T_2

Figure 10. Residual analysis of T_2 regression equation

Figure 9(a) shows the normal probability distribution of residual errors in the prediction model of bone grinding temperature T_1, which is the most ideal situation when the two are in a straight line. As can be seen from Figure 9(a), the predictive values are all distributed around the straight line. Figure 9(b) shows the relationship between predictive value and simulation value. The closer the point is to the straight line, the smaller the difference between the simulated value and the predicted value. It can be seen from Figure 9(b) that the prediction values are all close to the straight line.

Figure 10(a) shows the normal probability distribution of residual errors in the prediction model of bone grinding temperature T_2, As can be seen from Figure 10(a), the predictive values are all distributed around the straight line. Figure 10(b) shows the relationship between predictive value and simulation value. It can be seen from Figure 10(b) that the predictive values are all close to the straight line. According to the above analysis, the prediction models constructed are all reasonable.

Figure 11 is a response surface diagram of T_1 and T_2 with respect to rotating speed A, feed speed B, and grinding thickness C. Figure 11(a) is a three-dimensional response curve of the effect of rotating speed A and feed speed B on T_1, and Figure 11(b) is a three-dimensional response curve of the effect of rotating speed A and feed speed B on T_2. It can be seen from Figure 11(a) and Figure 11(b) that within the research range of the parameters, when the feed speed B of grinding tool is constant, the grinding temperature will increase with the increase of rotating speed A, and when the rotating speed A is constant, the grinding temperature will decrease with the increase of feed speed B. Therefore, regardless of whether coolant is used, the areas with the highest grinding temperatures are concentrated in the areas where the rotating speed A is high and the feed rate B is low. Comparing Figure 11, it can be found that the the coolant can reduce the grinding temperature of bone grinding.

Figure 11(c) is the three-dimensional response curve of the effect of rotating speed A and grinding thickness C on T_1, and Figure 11(d) is the three-dimensional response curve of the effect of rotating speed A and grinding thickness C on T_2. It can be seen from Figure 11(c) and Figure 11(d) that within the research range of parameters, when the rotating speed A is constant, the grinding temperature will increase with the increase of grinding thickness C. The temperature will increase as the rotating speed A increases. Therefore, regardless of whether the coolant is used or not, the areas with the highest grinding temperatures are concentrated in the areas where the rotating speed A is high and the grinding thickness C is large. Comparing Figure 11(c) with Figure 11(d), it can be found that the coolant can reduce the grinding temperature of bone grinding.

Figure 11(e) is the three-dimensional response curve of the influence of feed speed B and grinding thickness C on T_1, and Figure 11(f) is the three-dimensional response curve of the effect of feed speed B and grinding thickness C on T_2 ,It can be seen from Figure 11(c) and Figure 11(f) that within the research range of parameters, when the feed rate B is constant, the grinding temperature will increase with the increase of grinding thickness C, and when the grinding thickness C is constant, the grinding temperature decreases with the increasing of feed rate B. It can be seen from the above that the maximum area of grinding temperature is concentrated in the area where the grinding thickness C is larger and the feed speed B is smaller, regardless of whether the coolant is used or not. Comparing Figure 11(e) with Figure 11(f), it can be found that the coolant can reduce the grinding temperature of bone grinding.

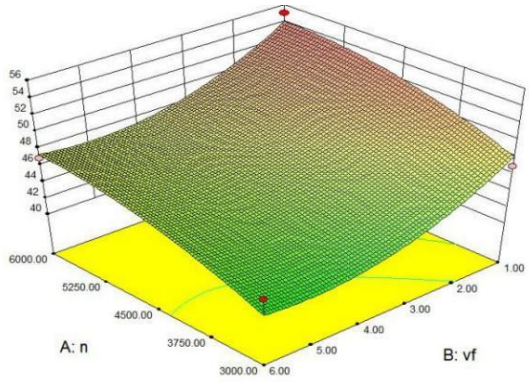

(a) The influence of rotating speed A and feed speed B on T_1

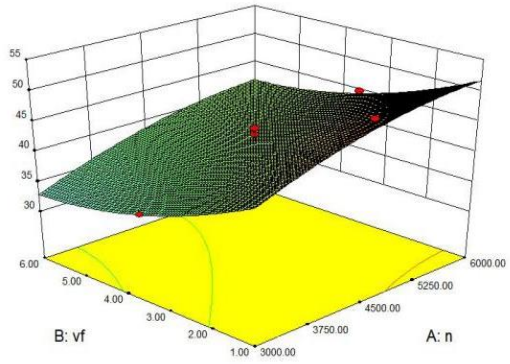

(b) The influence of rotating speed A and feed speed B on T_2

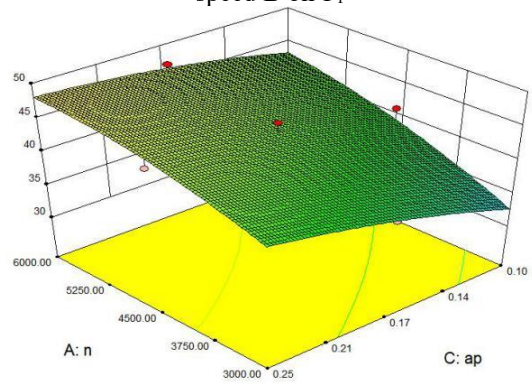

(c) The influence of rotating speed A and grinding thickness C on T_1

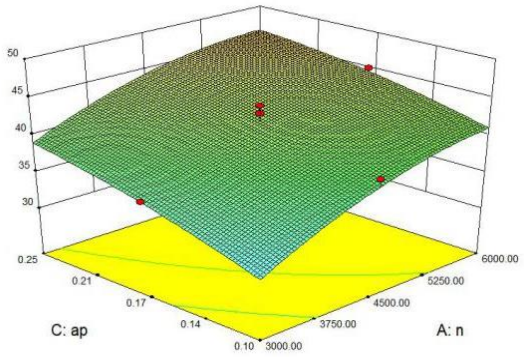

(d) The influence of rotating speed A and grinding thickness C on T_2

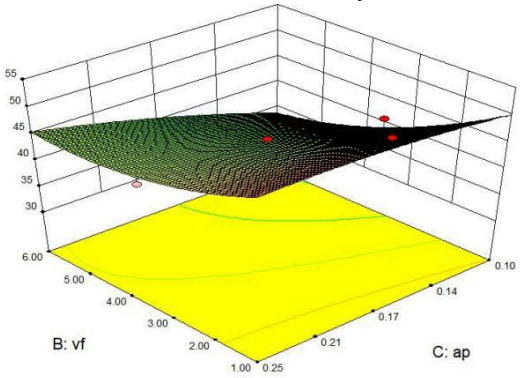

(e) The influence of feed speed B and grinding thickness C on T_1

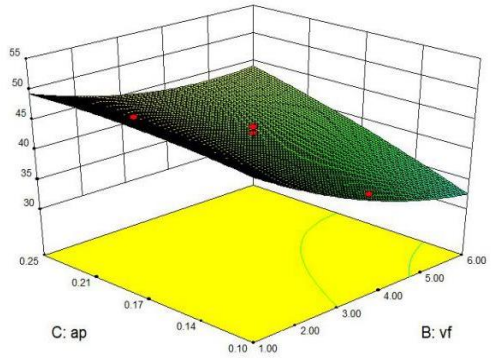

(f) The influence of feed speed B and grinding thickness C on T_2

Figure 11. Response surface diagram of T_1 and T_2 with respect to rotating speed A, feed speed B and grinding thickness C

Therefore, in the process of bone grinding, whether coolant is used or not, the grinding temperature is higher when the rotating speed A is higher, the grinding thickness C is larger and the feed speed B is slower, and the coolant in the grinding process can reduce the grinding temperature of bone grinding.

Figure 12 is a response surface diagram among grinding temperature T_2, convective heat transfer coefficient D and friction coefficient E. It can be seen from Figure 12 that when the convective heat transfer coefficient D is larger, the grinding temperature is lower, and when the friction coefficient E is larger, the grinding temperature is higher.

In conclusion, in bone grinding surgery, in order to reduce the grinding temperature, reduce the damage to bone cells and tissue, and improve the success rate of bone grinding surgery, the rotating speed A shall be low, the feed speed B shall be fast, the grinding thickness C shall be small, and the grinding fluid with large convection heat transfer coefficient D and small friction coefficient E shall be selected.

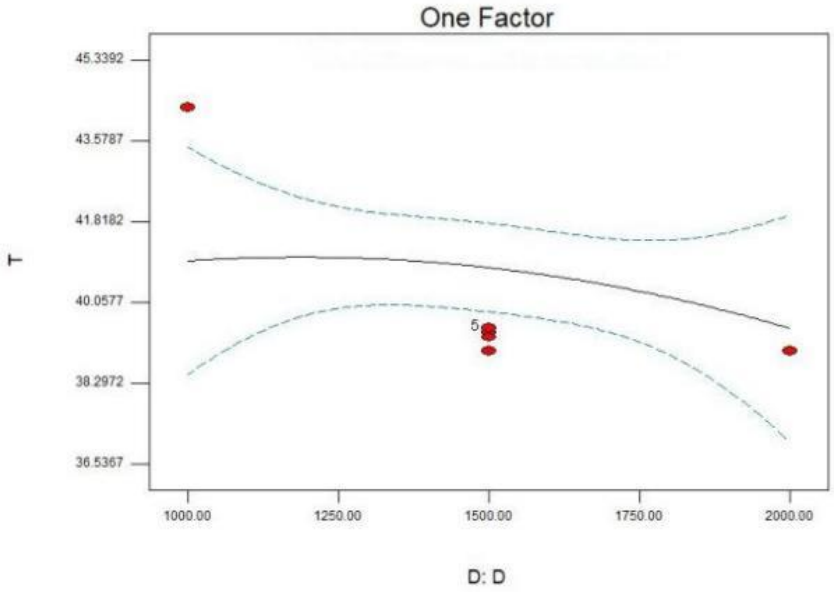

(a) Relationship between grinding temperature T_2 and convection heat transfer coefficient D

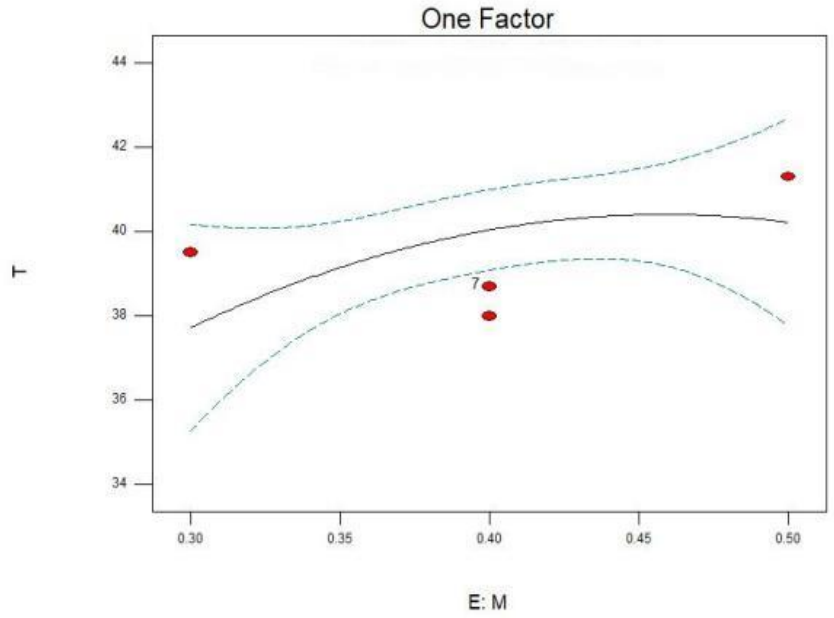

(b) Relationship between grinding temperature T_2 and friction coefficient E

Figure 12. Relationship among grinding temperature T_2, convective heat transfer coefficient D and friction coefficient E

3.4 Verification Experiment

The simulation value, predictive value and experimental value of grinding temperature when the normal saline was used, the rotating speed was 5000r/min, the grinding thickness was 0.1mm, and the feed speed was 2mm/s were compared and analyzed.

Figure 13 is the relationship figure between grinding temperature and rotating speed when normal saline is used. As can be seen from the figure, the trend of simulation value, predictive value and experimental value is basically the same when medical normal saline is used for grinding, that is, grinding temperature increases with the increase of rotating speed, and the correctness of simulation model and prediction model is verified through comparative analysis.

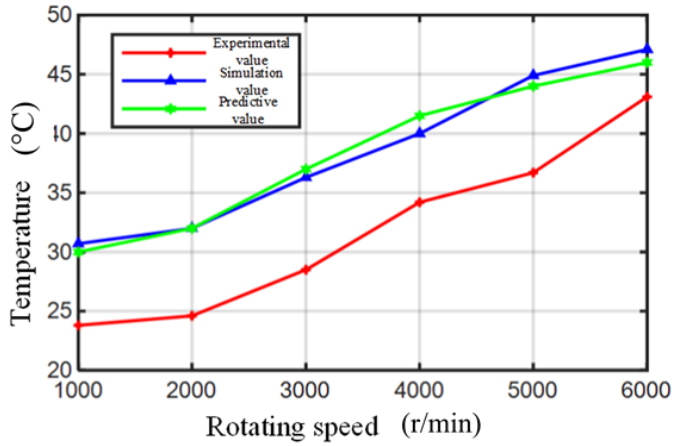

Figure 13. Relationship between grinding temperature and speed

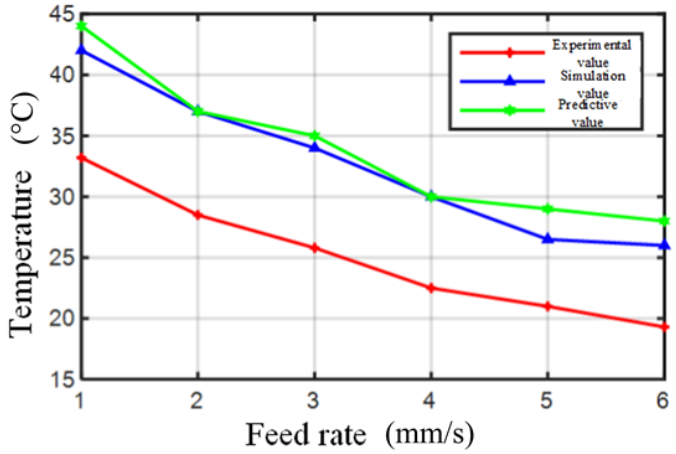

Figure 14. Relationship between grinding temperature and feed speed

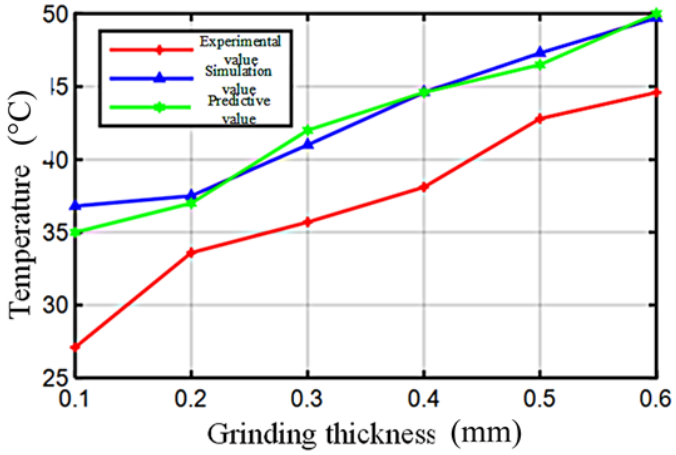

Figure 15. Relationship between grinding temperature and grinding thickness

Figure 14 is the relationship figure between grinding temperature and feed speed when medical normal saline is used. As can be seen from the figure, the trend of simulation value, predictive value and experimental value is basically the same when normal saline is used for grinding, that is, grinding temperature increases with the increase of feed speed, and the correctness of simulation model and prediction model is verified through comparative analysis.

Figure 15 is the relationship figure between grinding temperature and grinding thickness when normal saline is used. As can be seen from the figure, the trend of simulation value, predictive value and experimental value is

basically the same when normal saline is used for grinding, that is, grinding temperature increases with the increase of grinding thickness, and the correctness of simulation model and prediction model is verified through comparative analysis.

Through the above analysis, it can be found that the relationship between grinding temperature and grinding parameters obtained by simulation, prediction and experiment is consistent, and the accuracy of simulation model and prediction model can be verified by comparing the experimental value with simulation value and predictive value. Comparing the experimental results with the simulation results, it can be found that the grinding temperature in the experiment is relatively low, and the cooling effect of normal saline is more significant.

It can be seen form Figure 14 to Figure 15, there is a large error between the simulation value and the experimental value. The cause of production error is analyzed as follows: Firstly, because the simulation model established is a single abrasive grinding model, although the single abrasive model can simplify the simulation process, there is a certain gap between the grinding process and the actual grinding tool model, resulting in different grinding temperatures. Secondly, the internal structure of the bone is not considered in the simulation process. The bone material parameters are empirical parameters, which are different from the actual parameters. The experiment uses fresh bovine bone, and the difference between the simulation and experimental results caused by the difference of grinding materials. Finally, the measurement accuracy of the temperature sensor and the temperature of the external environment will also affect experimental result.

4. Conclusions

(1) The FE model of single abrasive bone grinding was established by using ABAQUS software. The influence of cooling and lubrication parameters on grinding temperature was investigated by changing convective heat transfer coefficient and friction coefficient in the simulation model.

(2) Response surface design of experiment was carried out to obtain the simulation results, and Design-Expert was used to establish a multiple regression prediction models of grinding temperature under different cooling and lubrication modes and without grinding fluid respectively. Variance analysis and response surface analysis of the prediction model of grinding temperature verified the effectiveness of the grinding simulation results.

(3) A robot bone grinding experiment platform was built, and the grinding temperature was measured by means of the thermocouple thermometer. The verification experiments of the influence of cooling and lubrication parameters on bone grinding temperature were performed when using normal saline and the simulation value, predictive value and experimental value of grinding temperature were consistent by compared.

Funding

This work was supported in part by the National Natural Science Foundation of China (Grant No.: 52275496) and the Natural Science Foundation of Shandong Province of China (Grant No.: ZR2020MF099).

Data Availability

The data used to support the findings of this study are available from the corresponding author upon request.

Conflicts of Interest

The authors declare that they have no conflicts of interest.

References

[1] P. P. Rao, “Robotic surgery: new robots and finally some real competition,” *World J. Urol.*, vol. 36, pp. 537-541, 2018. https://doi.org/10.1007/s00345-018-2213-y.

[2] D. J. Jacofsky and M. Allen, “Robotics in arthroplasty: a comprehensive review,” *J. Arthroplasty*, vol. 31, no. 10, pp. 2353-2363, 2016. https://doi.org/10.1016/j.arth.2016.05.026.

[3] M. B. Abouzgia and D. F. James, “Temperature rise during drilling through bone,” *Int J. Oral. Max. Impl.*, vol. 12, no. 3, pp. 342-353, 1997.

[4] V. Tahmasbi, M. Ghoreishi, and M. Zolfaghari, “Sensitivity analysis of temperature and force in robotic bone drilling process using Sobol statistical method,” Biotechnol. Biotec. Eq., vol. 32, no. 1, pp. 130-141, 2018. https://doi.org/10.1080/13102818.2017.1403863.

[5] L. L. Xu, C. Y. Wang, M. Jiang, H. Y. He, Y. X. Song, H. Y. Chen, J. N. Shen, and J. Y. Zhang, “Drilling force and temperature of bone under dry and physiological drilling conditions,” Chinese J. Mech. Eng., vol. 27, pp. 1240-1248, 2014. https://doi.org/10.3901/CJME.2014.0912.151.

[6] G. Augustin, S. Davila, T. Udilljak, T. Staroveski, D. Brezak, and S. Babic, “Temperature changes during cortical bone drilling with a newly designed step drill and an internally cooled drill,” Int. Orthop., vol. 36, pp. 1449-1456, 2012. https://doi.org/10.1007/s00264-012-1491-z.
[7] H. Kirschner and W. Meyer, “Entwicklung einer innenkühlung für chirurgische bohrer,” *DtschZahnaztlZeitschrift*, vol. 30, no. 7, pp. 436-438, 1975.
[8] S. Gholampour and H. H. H. Deh, “The effect of spatial distances between holes and time delays between bone drillings based on examination of heat accumulation and risk of bone thermal necrosis,” *Biomed. Eng. Online*, vol. 18, pp. 1-14, 2019. https://doi.org/10.1186/s12938-019-0686-6.
[9] H. H. Hassanalideh and S. Gholampour, “Finding the optimal drill bit material and proper drilling condition for utilization in the programming of robot-assisted drilling of bone,” *CIRP J. Manuf. Sci. Technol.*, vol. 31, pp. 34-47, 2020. https://doi.org/10.1016/j.cirpj.2020.09.011.
[10] S. Kondo, Y. Okada, H. Iseki, T. Hori, K. Takakura, A. Kobayashi, and H. Nagata, “Thermological study of drilling bone tissue with a high-speed drill,” *Neurosurgery*, vol. 46, no. 5, pp. 1162-1168, 2000. https://doi.org/10.1097/00006123-200005000-00029.
[11] H. C. Shin and Y. S. Yoon, “Bone temperature estimation during orthopaedic round bur milling operations,” *J. Biomech.*, vol. 39, no. 1, pp. 33-39, 2006. https://doi.org/10.1016/j.jbiomech.2004.11.004.
[12] M. Yang, C. H. Li, Y. B. Zhang, Y. G. Wang, B. K. Li, D. Z. Jia, Y. L. Hou, and R. Z. Li, “Research on microscale skull grinding temperature field under different cooling conditions,” Appl. Therm. Eng., vol. 126, pp. 525-537, 2017. https://doi.org/10.1016/j.applthermaleng.2017.07.183.
[13] H. Q. Tian, C. L. Zheng, C. C. Wang, J. Li, and Y. N. Yao, “Modeling and simulation of a single abrasive grain micro-grinding force and temperature of bone,” *J. Biomech. Sci. Eng.*, vol. 15, no. 4, pp. 1-12, 2020. https://doi.org/10.1299/jbse.20-00012.
[14] Q. W. Wang, H. Q. Tian, X. Q. Dang, J. B. Pan, Y. Gao, Q. Xu, Z. Lin, and Y. Yao, “Temperature distribution simulation, prediction and sensitivity analysis of orthogonal cutting of cortical bone,” *Part H: J. Eng. Med.*, vol. 236, no. 1, pp. 103-120, 2022. https://doi.org/10.1177/09544119211049869.
[15] K. Alam, A. V. Mitrofanov, and V. V. Silberschmidt, “Thermal analysis of orthogonal cutting of cortical bone using finite element simulations,” *Int. J. Exp. Com. Biomech.*, vol. 1, no. 3, pp. 236-251, 2010. https://doi.org/10.1504/IJECB.2010.035259.
[16] T. P. Ng and S. Koloor, “Mechanical behavior of cortical bone,” *Trauma Plat. Sys.*, vol. 2017, pp. 19-31, 2017.
[17] D. Remache, M. Semaan, J. M. Rossi, M. Pithioux, and J. L. Milan, “Application of the Johnson-Cook plasticity model in the finite element simulations of the nanoindentation of the cortical bone,” J. Mech. Behav. Biomed., vol. 101, Article ID: 103426, 2020. https://doi.org/10.1016/j.jmbbm.2019.103426.
[18] M. Ghoreishi and V. Tahmasbi, “Optimization of material removal rate in dry electro-discharge machining process,” Modares Mech. Eng., vol. 14, no. 12, pp. 9-18, 2015.
[19] T. H. Hou, C. H. Su, and W. L. Liu, “Parameters optimization of a nano-particle wet milling process using the Taguchi method, response surface method and genetic algorithm,” *Powder Technol.*, vol. 173, no. 3, pp. 153-162, 2007. https://doi.org/10.1016/j.powtec.2006.11.019.
[20] D. C. Montgomery, Design and analysis of experiments, New York, NY, USA: Wiley, 2008.